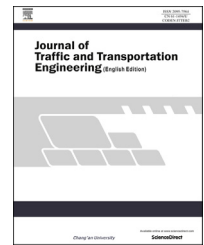


HOSTED BY

Available online at www.sciencedirect.com

ScienceDirect

journal homepage: www.elsevier.com/locate/jtte

Original Research Paper

Calculation of skid resistance from texture measurements



Andreas Ueckermann*, Dawei Wang, Markus Oeser, Bernhard Steinauer

Institute of Highway Engineering, RWTH Aachen University, Aachen 52056, Germany

ARTICLE INFO

Article history:

Available online 14 January 2015

Keywords:

Skid resistance
Contactless measurement
Pavement texture
Rubber friction model

ABSTRACT

There is a wide range of routine skid resistance measurement devices on the market. All of them are measuring the friction force between a rubber wheel and the wetted road surface. Common to all of them is that they are relatively complex and costly because generally a truck carrying a large water tank is needed to wet the surface with a defined water layer. Because of the limited amount of water they can carry they are limited in range. Besides that the measurement is depending on factors like water film thickness, temperature, measurement speed, rubber aging, rubber wear and even road evenness and curviness. All of these factors will affect the skid resistance and are difficult to control. We present a concept of contactless skid resistance measurement which is based on optical texture measurement and consists of two components: measurement of the pavement texture by means of an optical measuring system and calculation of the skid resistance based on the measured texture by means of a rubber friction model. The basic assumptions underlying the theoretical approach and the model itself based on the theory of Persson are presented. The concept is applied to a laboratory device called Wehner/Schulze (W/S) machine to prove the theoretical approach. The results are very promising. A strong indication could be provided that skid resistance could be measured without contact in the future.

© 2015 Periodical Offices of Chang'an University. Production and hosting by Elsevier B.V. on behalf of Owner. This is an open access article under the CC BY-NC-ND license (<http://creativecommons.org/licenses/by-nc-nd/4.0/>).

1. Introduction

Wet road skid resistance is an important functional property of road pavements. Pavements are designed to offer a safe ride to the road users under different climatic conditions and over a long service life. In order to maintain a sufficient level of skid resistance pavement monitoring is performed at regular intervals.

All of the measurement devices in use are based on the principle of rubber friction; generally, the friction force between a measuring wheel, operated at a defined speed, vertical load and transversal slip, and the pavement is measured. Those measurement devices are relatively complex and costly because in most cases a truck carrying a large water tank is needed to wet the surface with a defined layer of water. Because of the limited amount of water they can carry they are limited in range. Besides that the measurement is depending

* Corresponding author. Tel.: +49 241 80 26744; fax: +49 241 80 22141.

E-mail address: ueckermann@isac.rwth-aachen.de (A. Ueckermann).

Peer review under responsibility of Periodical Offices of Chang'an University.

<http://dx.doi.org/10.1016/j.jtte.2015.01.001>

2095-7564/© 2015 Periodical Offices of Chang'an University. Production and hosting by Elsevier B.V. on behalf of Owner. This is an open access article under the CC BY-NC-ND license (<http://creativecommons.org/licenses/by-nc-nd/4.0/>).

on factors like water film thickness, temperature, measurement speed, rubber aging and wear and even road evenness and curviness. All of these factors will affect the skid resistance and are difficult to control.

For this reason several efforts have been undertaken in the past to predict skid resistance solely from optical texture measurements. Optical sensors are comparably cheap and easy to combine with existing measurement equipment for monitoring purposes. They are independent of rubber properties and the influence of an interfacial water film.

However, most of the approaches failed. One of the mistakes was to exclude the rubber properties from the approach. Another reason was that the resolution of the texture measurements was not high enough to capture the geometrical features governing the rubber friction.

This paper is intended to make a contribution to contactless skid resistance measurement. It deals with the prediction of skid resistance from texture measurements using a rubber friction model. The approach, the investigations and results are presented below. To begin with a brief literature review on contactless skid resistance measurement and factors influencing skid resistance shall be given.

2. Existing approaches and factors influencing skid resistance

Recent advances on contactless skid resistance measurement are reported by Dunford (2008, 2010) where skid resistance is predicted from parameters directly extracted from images of the road surface. Many approaches use 2-dimensional or 3-dimensional topographical data of the surface collected by means of laser displacement sensors or laser profile scanners (Mu et al., 2003; Kebrle and Walker, 2007; Xie et al., 2008; Meegoda, 2009; Cigada et al., 2010; Goubert et al., 2010). Topographical data can also be generated by stereoscopic imaging. Although not new in the application to pavement texture analysis (Sabey and Lupton, 1967; Schonfeld, 1970) recent work on algorithms for the extraction of surface topography from image and the assessment of surface roughness by means of image-based descriptors is described (Ben Slimane et al., 2008; Xie et al., 2009; El Gendy et al., 2011). Light scattering methods based on depolarization (Spring III and King, 1981; Wambold et al., 1982) or back-scattering pattern analysis (Kazakov, 1986; Iaquina and Fouilloux, 2003) have been proposed in the past but obviously not pursued, presumably because optical pavement properties not necessarily reflect tire-pavement interaction.

Basically, three approaches to predict skid resistance from road surface data can be found in literature: prediction through texture or texture-related parameters, which correlate with rubber friction, prediction through modeling of rubber contact and rubber friction (partially including the lubricant), and a combined approach comprising both texture indicators and physical modeling as described in previous studies (Do et al., 2004a, 2004b; Do and Zahouani, 2005; Kane and Do, 2006). The first approach can involve statistical regression models (Zahouani et al., 2000; Ergün et al., 2005; Shalaby and El Gendy, 2008; Schulze, 2011), fuzzy-logic (Ustuntas, 2007) and artificial neural networks (Kebrle and

Walker, 2007; Xie et al., 2008; Wang et al., 2012). The second one largely focuses on hysteresis friction since hysteresis is the dominating mechanism during braking on wet road pavements. However, other phenomena like adhesion and the influence of water in the tyre/road interface are dealt with as well in related papers.

It is widely acknowledged that the microtexture (wavelengths below 0.5 mm) governs the peak value of the wet friction coefficient-slip (or sliding speed) curve whereas the macrotexture (wavelengths between 0.5 and 50 mm) governs its decrease. The lower the macrotexture the steeper the decrease. A high macrotexture (i.e. a high water drainage capacity) can improve the skid resistance over a wide range of speeds. Pioneering studies on the role of micro/macrotexture under wet braking conditions can be found (Giles, 1957, 1965; Schulze, 1959, 1969, 1970; Moore, 1969, 1975; Geyer, 1972; Holla and Yandell, 1973; Moore and Humphreys, 1973; Balmer, 1975; Rhode, 1976; Holla, 1977; Taneerananon and Yandell, 1981; Holt and Musgrove, 1982; Horne and Bühlmann, 1983). Size, density and shape (slope) of the microasperities on top of the aggregates are essential to overcome the thin water film and to make direct contact with the rubber. A close relationship between friction coefficient and average slope of the microasperities in the contact zone can be observed and mathematically explained (Yandell, 1971; Forster, 1981; Pinnington, 2009). More recent approaches to define texture descriptors relevant to skid resistance can be found (Zahouani et al., 2000; Ergün et al., 2005; Shalaby and El Gendy, 2008; Schulze, 2011) as mentioned above. Other researchers emphasize the fractal nature of pavement texture and use a fractal or spectral description of the self-affine road surface (Majumdar and Bhushan, 1990; Majumdar and Tien, 1990; Radó, 1994; Kokkalis and Panagouli, 1998; Klüppel and Heinrich, 2000; Persson et al., 2001). Instead of a truncated Fourier series a combination of a Fourier series and a Weierstrass–Mandelbrot series is used (Radó, 1994; Pinnington, 2012), amongst others to allow for the asymmetry of worn pavement surfaces. Recent theories on rubber friction (Klüppel and Heinrich, 2000; Persson et al., 2001) assume a smooth rubber surface and a rigid substrate with a self-affine surface roughness that is described by the power spectral density or the height-difference correlation function. Two and three parameters respectively are needed to describe the texture. Close relationships between these parameters and wet tire traction have been observed (Heinrich, 1992a, 1992b).

When skid resistance is measured, let's say with a measuring speed of 60 km/h and a fixed slip of 20%, only a part of the measured slip speed, which would be 12 km/h, is due to actual sliding, the other one is due to deformation of the tread elements. The amount of deformation slip depends on the tire stiffness: a blank, "stiff" tire would exhibit only little deformation implying that the measured slip speed almost equals the actual slip speed, whereas a treaded tire would undergo a higher deformation, depending on the elasticity of the tread rubber and the geometry of the tread pattern. In most cases the slip measured is just a mean value averaged over the contact length and thus a simplification of the real slip conditions within the contact area.

A three-zone model according to Moore (1966) can help to illustrate the contact conditions in the tire-road interface

during rolling or skidding on a wet surface from a tribology point of view. The “sinkage” or “squeeze-film” zone is the first zone when the tyre enters the contact patch. It corresponds to the “elasto-hydrodynamic lubrication” regime where the water completely separates the two surfaces. The sinkage zone is followed by the “draping” or “transition” zone. It corresponds to the “mixed lubrication” regime where the tread elements, having penetrated the squeeze-film, commence to “drape” over the major asperities. The draping zone is followed by the actual contact or traction zone which corresponds to the “boundary lubrication” regime where in parts dry contact can be established. The lengths of the zones depend on vehicle speed and the amount of water that has to be expelled from the interface. Due to partly the lubricant and partly the sliding velocity used in skid resistance measurements adhesion is largely inhibited and hysteretic friction dominates friction mechanism (Klüppel and Heinrich, 2000; Persson et al., 2001).

Several models have been derived in the past to describe the influence of the lubricant on the friction coefficient (Moore, 1966; Schulze, 1979; Golden, 1981; Taneerananon and Yandell, 1981; Horne and Bühlmann, 1983; Yandell et al., 1983). Empirical approaches used within the context of harmonizing skid resistance measurements include the water influence indirectly by an exponential function characterized by a speed factor which again is dependent on the macro-texture. Different functions have been proposed to describe the speed dependence (Leu and Henry, 1978; Radó, 1994; Wambold et al., 1995; La Torre and Domenichini, 2001; Descornet and Schmidt, 2006), and more recently the function is derived from the Stribeck curve which describes the friction as a function of speed or a lubrication parameter in different lubrication regimes (Do et al., 2004a, 2004b).

In spite of the extensive knowledge on the relationship between pavement texture and wet skid behavior gained over the past decades, a reliable method to predict skid resistance solely from texture measurements is still missing.

3. Rubber friction

Rubber friction is the predominant physical phenomenon behind skid resistance measurements. It involves several components (Kummer, 1968; Geyer, 1972): 1) the hysteretic component which results from internal friction of the rubber. During sliding over a rough surface the asperities exert oscillating forces on the rubber resulting in energy dissipation due to internal damping of the rubber. Grosch (1963) found the energy dissipation to be coupled with characteristic length scales of the substrate, confirming that the texture is a main factor inducing friction; 2) the adhesion component which results from attractive binding forces between the rubber surface and the substrate. It is important only for clean, smooth surfaces and small sliding velocities. Schallamach (1953) assigned adhesion friction to an intrinsic length scale of the rubber, i.e. the distance a rubber chain end jumps forward during sliding. Persson (2000) attributed adhesion friction to the roughness of the substrate as well and argued that even smooth surfaces (like glass) are not smooth on nanoscales. He showed that, due to the low elastic modulus, the interfacial free energy forces the rubber

to fill out the cavities on a nano-scale, leading to oscillating forces on the rubber during sliding. Klüppel and Heinrich (2000) adopted this view of “adhesion induced hysteretic friction” in their theory of rubber friction on self-affine road tracks; 3) the cohesion component of rubber friction which represents the energy required to produce new surfaces. It is associated with grooving of the rubber and abrasive wear; 4) the viscous friction component which arises from shearing of a viscous layer between tire and road surface. It can occur only on wet roads. The shearing generates a hydrodynamic pressure that tends to lift the tire from the pavement leading to an increased hydroplaning risk depending on the speed and water film thickness. Hysteresis and adhesion have been identified to contribute most to rubber friction (Kummer and Meyer, 1960; Greenwood et al., 1961; Savkoor, 1965; Bowden and Tabor, 1966; Kummer, 1966; Ludema and Tabor, 1966; Tabor, 1967; Moore, 1972, 1980; Moore and Geyer, 1974; Barquins, 1985; Barquins and Roberts, 1986; Roberts, 1992).

In recent years extensive work has been done, namely by Persson et al. on mathematical models which allow to quantitatively determine the kinetic friction coefficient of rubber sliding against a hard, rough substrate (Le Gal and Klüppel, 2008; Heinrich et al., 2000; Klüppel and Heinrich, 2000; Persson, 2001a, 2001b). The theories focus on the hysteresis component of rubber friction but adhesion can optionally be included. The models have been extended to include tire dynamics as well (Heinrich and Klüppel, 2008; Persson, 2011a, 2011b). Other phenomena like anisotropy of surface texture (Carbone et al., 2009), role of the flash temperature (Persson, 2006a, 2006b), heat transfer between the elastic solid and the rough surface (Persson et al., 2010), interfacial separation (Persson, 2007; Yang and Persson, 2008) and the influence of water in the rubber/substrate interface in terms of sealing effect (Persson et al., 2004, 2005) and squeeze-out (Persson, 2011a, 2011b) have been treated as well.

Both Persson's model and the model of Heinrich and Klüppel have a physical foundation and need input information about the complex modulus of the rubber, the statistical roughness of the substrate, the contact pressure, sliding speed and temperature. The general approach is quite similar. However, Heinrich and Klüppel use a contact model based on the theory of Greenwood and Williamson (1966) which they extended to multiple-scale roughness surfaces while Persson developed a new three-dimensional contact mechanics theory (Persson, 2006a, 2006b) which can be applied to elasto-plastic contact as well. Both models consider the surface roughness on multiple length scales and thus need the viscoelastic properties of the elastomer to be known over a wide frequency range. Heinrich and Klüppel calculate the hysteresis friction coefficient based on a two-dimensional approach while Persson's model is fully 3D and based on three-dimensional data (i.e. the pavement surface). It takes into account how the rubber, on each length scale, is able to follow the hard substrate. The predictive capabilities of both models have been investigated (Westermann et al., 2004) by comparing the results with friction experiments. Good agreement was found. The results demonstrate that the “flash” temperatures (local hot spots) need to be considered for dry friction prediction.

4. Persson's model of rubber friction

The model used for the prediction of skid resistance is based on the theory of Persson. Because road surfaces are relatively rough and skid resistance is measured under wet conditions and comparatively high sliding velocities the adhesion component can be neglected and hysteresis is considered to be dominating friction mechanism. In the following the theory of Persson is summarized in terms of the key equations. For a deeper understanding of the underlying assumptions we refer to the original papers (Persson, 2001a, 2001b).

The kinetic coefficient of friction (μ_k) under steady-state conditions is the result of hysteresis contributions from multiple scales of roughness as expressed by the following equations

$$\mu_k = \frac{1}{2} \int_{q_L}^{q_1} q^3 C(q) P(q) dq \int_0^{2\pi} \cos(\phi) \text{Im} \left(\frac{E(qv \cos(\phi))}{(1-\nu^2)\sigma_0} \right) d\phi \quad (1)$$

$$P(q) = \frac{2}{\pi} \int_0^{\infty} \frac{\sin(x)}{x} \exp(-x^2 G(q)) dx = \text{erf} \left(\frac{1}{2\sqrt{G(q)}} \right) \quad (2)$$

$$G(q) = \frac{1}{8} \int_{q_L}^q q^3 C(q) dq \int_0^{2\pi} \left| \frac{E(qv \cos(\phi))}{(1-\nu^2)\sigma_0} \right|^2 d\phi \quad (3)$$

$$\lambda = 2\pi/q \quad (4)$$

$$q = (q_x, q_y) = (q \cos(\phi), q \sin(\phi)) \quad (5)$$

where q is the spatial angular frequency or magnitude of the wave vector corresponding to the wavelength λ , q_L is the lower integration limit where L is of order the length of a tread block, q_1 is the upper cut-off frequency corresponding to a short distance cut-off wavelength which is depending on the operating conditions such as road contamination, wet or dry friction, measuring velocity and amount of water that has to be expelled from the interface. For dry friction the short distance wavelength can be of order one micrometer. However, surface contamination like dust and rubber particles will determine the smallest wavelength since the rubber cannot penetrate into surface cavities smaller than the typical particle diameter (Persson, 2001b). On a wet surface the short distance cut-off wavelength is determined by the smallest asperities which can penetrate the water film and the size of water "pools" trapped in small surface cavities.

The function $C(q)$ denotes the two-dimensional power spectral density (PSD) of the pavement surface

$$C(q) = \frac{1}{(2\pi)^2} \int h(x) h(0) e^{-iqx} dx \quad (6)$$

where $h(x)$ is the surface height measured from the average plane with $x = (x, y)$ and $h = 0$. The statistical properties of the texture are assumed to be isotropic so that $C(q)$ only depends on the magnitude $q = |q|$ of the wave vector q . A typical example for a road surface is shown in Fig. 1. Many roughness spectra exhibit fractal properties, that is, their power spectral

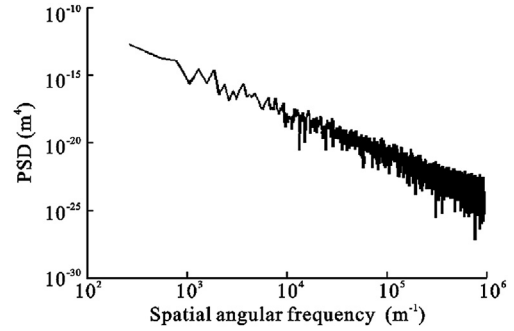


Fig. 1 – Two-dimensional power spectral density of a pavement surface.

density can be characterized by a straight line in the log–log scale. Via the sliding velocity v , frequencies $f = qv \cos(\phi)$ are excited which act on the tread block and depend on the sliding direction which is given by the angle ϕ between sliding direction and particular wave vector. They determine the material behavior via the loss modulus $\text{Im}(E(qv \cos(\phi)))$ in the "friction" Eq. (1) and the absolute value $|E(qv \cos(\phi))|$ in Eq. (3) which determines the contact conditions during sliding.

Fig. 2 shows the frequency dependent modulus of rubber schematically in terms of its storage (red) and loss modulus (blue). For low frequencies the rubber is relatively soft. With increasing frequency it stiffens and finally reaches a maximum which in this case exceeds the low-frequency stiffness by a factor of 200 (in case of the storage modulus). In the transition zone the loss tangent ($\text{Im}(E)/\text{Re}(E)$) passes through its maximum (not shown). This is where the most energy is dissipated. σ_0 is the macroscopic contact pressure and ν Poisson's ratio which for rubber can be set to 0.5.

The contact function $P(q) = A(q)/A_0$ describes the ratio of real and nominal (macroscopic) area of contact where contact occurs when the surfaces are smoothed on spatial frequencies higher than q . Via Eq. (3) $P(q)$, again, is dependent on the contact pressure, the sliding velocity, the surface texture $C(q)$ and the material properties of the rubber (Young's modulus and Poisson's ratio). The real contact area $A(q)$ normally is only a fraction of the macroscopic contact area because contact only occurs on the top of the surface asperities. The top of an asperity, in turn, would reveal many small-scale asperities if observed under magnification which in turn would exhibit even tinier asperities. $P(q)$ accounts for this

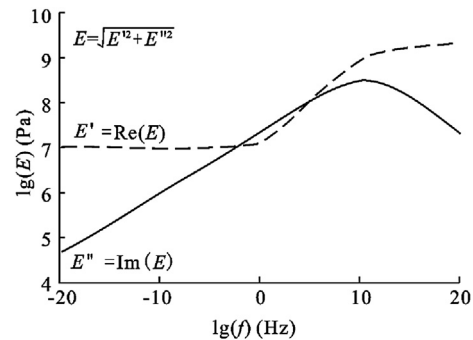


Fig. 2 – Loss and storage modulus of rubber (schematic).

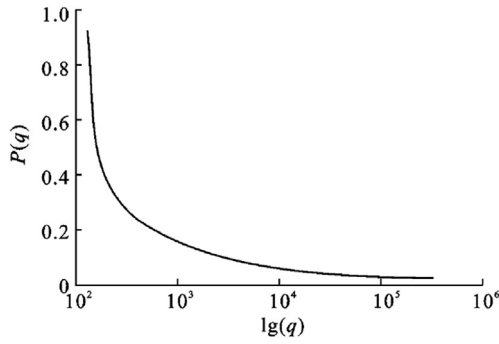


Fig. 3 – Normalized area of contact $P(q)$ as a function of the spatial angular frequency q .

scale dependent or fractal behavior. An example of a contact function $P(q)$ is given in Fig. 3.

We conclude that the friction coefficient according to Eqs. (1)–(3) is the result of hysteresis contributions from a wide band of frequencies q limited by the smallest asperities the rubber can follow on the one hand and the size of a tread block on the other hand. It is dependent on the contact pressure, the sliding velocity, the surface texture and the material properties of the rubber (Young’s modulus and Poisson’s ratio).

In case of dry friction the so-called flash temperatures have to be considered. Fig. 4 shows an infrared photograph of a tire as it is leaving the contact patch. The red and yellow colors indicate hot spots arising from tire-pavement contact. The temperatures are highest at the micro-asperity contact points and decrease radially from there. The hot spots are a function of time and location and overlap thermally with other micro-asperity contact regions in the vicinity. Besides that they are thermally coupled over many length scales. For surfaces with roughness on many length scales the temperature will increase with increasing magnification of the heat source. Persson describes the scale-dependent behavior by a temperature function $T(q)$ by analogy with the contact function $P(q)$ (Persson, 2006a, 2006b).

The deduction of $T(q)$ is based on the heat equation

$$\frac{\partial T}{\partial t} - D \nabla^2 T = \frac{Q(x, t)}{\rho C_V} \tag{7}$$

where Q is the energy production per unit volume and time arising from hysteresis friction of the rubber, D is the heat



Fig. 4 – Infrared photograph of a tire leaving the contact patch.

diffusivity, ρ is the mass density, C_V is the specific thermal capacity.

The key equations for the evaluation of the flash temperatures are given below. For a deeper understanding of the underlying assumptions we refer to the original paper (Persson, 2006a, 2006b).

$$T(q) = T_0 + \int_0^\infty g(q, q') f(q') dq' \tag{8}$$

with

$$f(q) = \frac{v q^4}{\rho C_V} C(q) \frac{P(q)}{P(q_m)} \int \cos(\phi) \text{Im} \frac{E(qv \cos(\phi), T(q))}{1 - \nu^2} d\phi \tag{9}$$

and

$$g(q, q') = \frac{1}{\pi} \int \frac{1}{D k^2} (1 - e^{-D k^2 t_0}) \frac{4 q'}{k^2 + 4 q'^2} \frac{4 q^2}{k^2 + 4 q^2} dk \tag{10}$$

where T_0 denotes the background temperature q is the spatial angular frequency and v the sliding velocity, $t_0 \approx R/v$, is about half the time the rubber is in contact with a macro-asperity of typical (average) radius R , q_m is the corresponding angular frequency of the macro-asperities, the function f represents the energy production term whereas the function g describes its decay into the solid. Note that the visco-elastic modulus is depending on the temperature $T(q)$ and the temperature, in turn, on the visco-elastic modulus. For unfilled rubber the Williams–Landel–Ferry (WLF) equation can be used to approximately describe the temperature dependence of $E(\omega, T)$ (Williams et al., 1955)

$$E(\omega, T) = E(\omega a_T / a_{T_0}, T_0) \tag{11}$$

$$\lg(a_T) = \frac{-8.86(T - T_g - 50)}{51.5 + T - T_g} \tag{12}$$

The shift factor a_T determines the shift of the master curve towards increasing frequencies for increasing temperatures. It is valid for temperatures T greater than the glass transition temperature T_g . Fig. 5 qualitatively demonstrates the influence of temperature on the modulus of elasticity.

In Fig. 6 the flash temperatures $T(q)$ calculated according to Eq. (8) for a rubber sliding with a constant speed over a rough hard substrate are shown. On a macroscopic scale the temperature in the rubber corresponds to the background

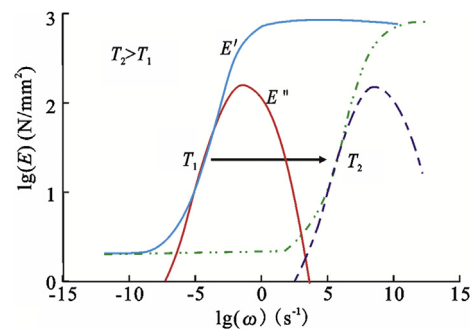


Fig. 5 – Effect of temperature increase on the modulus of elasticity.

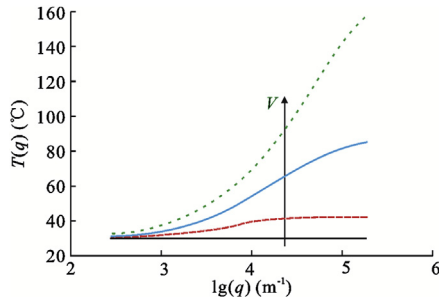


Fig. 6 – Flash temperatures $T(q)$ for different sliding velocities.

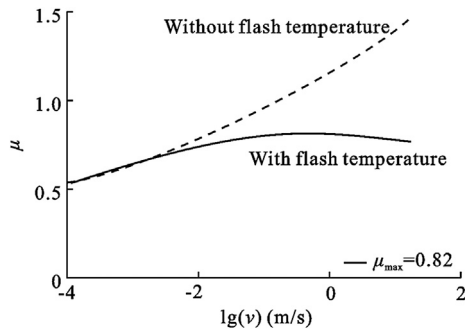


Fig. 7 – Friction coefficient as a function of sliding velocity with and without flash temperature.

temperature T_0 (30 °C in that particular case). With increasing magnification the temperatures $T(q)$ in the micro-asperity contact regions increase. The increase is depending on the sliding velocity (v): the higher the velocity the higher the energy production and hence the increase in temperature.

Fig. 7 demonstrates the influence of the flash temperature on the friction coefficient for an example calculation. Without flash temperature the coefficient of friction would rise progressively with increasing speed and according frequency because the excitation spectrum would be shifted towards higher hysteresis losses in the rubber. With the flash temperature considered the friction coefficient-sliding speed curve exhibits a degressive shape featuring a maximum and a subsequent decline in this example. Here, the friction curve is the result of two opposing effects: the effect due to the increase in velocity is reversed by the effect due to the increase

in (flash) temperature which shifts the viscoelastic modulus towards lower hysteresis losses and causes a decrease of the friction coefficient for high sliding velocities.

5. Concept of contactless skid resistance measurement

The traction between tire and road pavement amongst other things is depending on five major influencing factors: 1) the vehicle (axle load distribution, split-up of brake power, center of gravity, wheel alignment etc.); 2) the tire (dimension, construction, material, tread depth, tread design, inflation pressure, tire temperature etc.); 3) the driving mode (braking, acceleration, cornering, speed, ambient temperature etc.); 4) the surface conditions (dry, wet, water depth, contamination, snow, ice etc.); 5) the pavement (material, microtexture, macrotexture, drainage capacity etc.).

In Fig. 8(a) a typical deceleration curve from an ABS braking test on a wet road surface is shown. After a short transition phase a constant deceleration of, in this case, 9 m/s^2 is reached. Neglecting air, rolling and climbing resistance as well as the influence of rotating masses of wheels, engine and transmission and assuming that the traction potential at the front and rear axle is fully exploited we could draw a direct connection between the deceleration reached and the traction potential of a road/tire combination. Indeed, the traction potential would reduce to $\mu_{\text{wet}} = a/g$ with “ a ” being the deceleration and “ g ” the acceleration of gravity. We could call it the traction potential “of the road” or the skid resistance of the road since this would mark the optimum traction an “ideal” vehicle could achieve under the given influencing factors tire, driving mode and surface condition as described above. We can go further and notice that in this particular case the complex dynamic system reduces to a single mass or rather a rubber block sliding on the pavement surface as demonstrated in Fig. 8(b).

This analogy brings us to the idea that the traction potential of a pavement-alias its skid resistance-could be calculated by means of a rubber friction model. In a further step this would lead to the following concept of contactless skid resistance measurement as shown in Fig. 9, 1) measurement of the pavement texture by means of an optical measuring system and; 2) calculation of the traction potential-alias skid resistance-based on the measured texture by means of a rubber friction model.

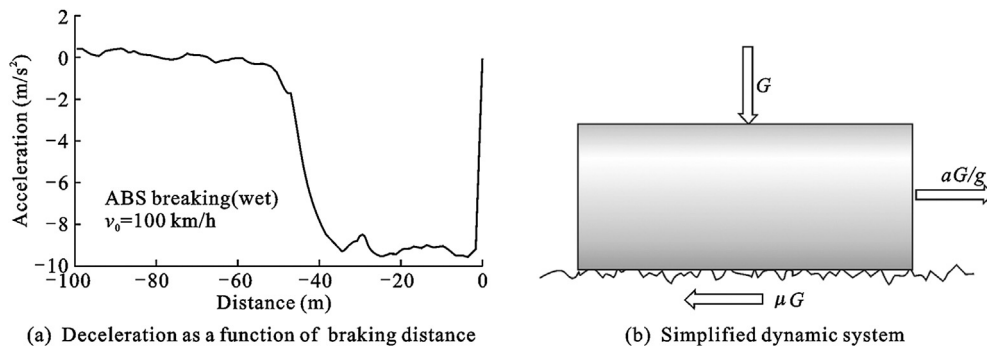


Fig. 8 – Dynamic system.

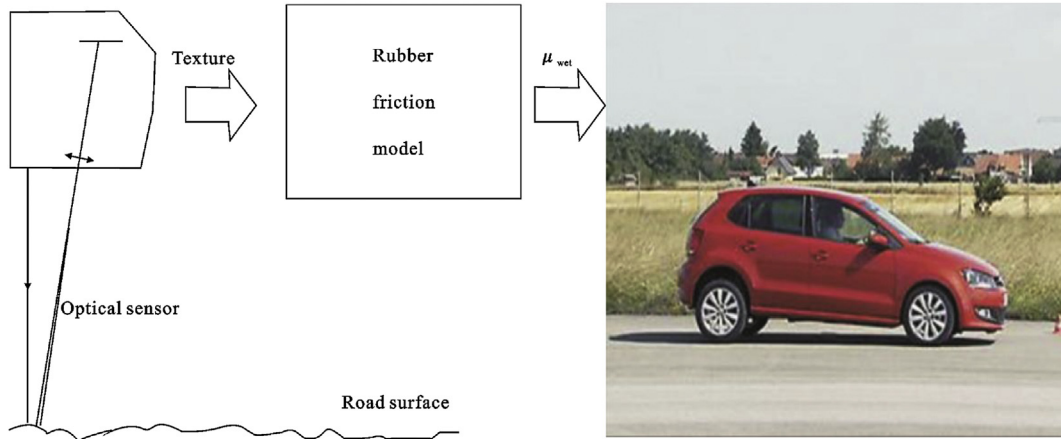


Fig. 9 – Concept of contactless skid resistance measurement.

When we look at the deceleration curve in Fig. 8, we can observe that the deceleration is virtually constant in the zone where it has reached its maximum, in this case over a distance of 35 m. This does not necessarily reflect the homogeneity of the pavement surface. In fact, the reason for this behavior which is not untypical for ABS braking is that the braked tire sort of “averages” or “integrates” along the braking path. This means that although locally the surface characteristics might be rather inhomogeneous the performance of the pavement (e.g. in terms of the achievable braking distance) might appear homogeneous because it is the result of a sequence of pavement–tire interactions accumulated over a certain length of the road. The measurement of skid resistance hence should be based on multiple measurements along the measuring path rather than on a single (local) measurement as illustrated in Fig. 10. A characteristic sampling or averaging length might cover a length of 30 m–40 m typical for braking distances.

6. Assumptions underlying the experimental approach

The concept of contactless skid resistance measurement is applied to a laboratory device called Wehner/Schulze (W/S) machine to prove the theoretical approach. The W/S-device



Fig. 10 – Measurement of skid resistance based on multiple measurements.

corresponds to a blocked-wheel braking test at a speed of 60 km/h and is described in the next chapter. The following assumptions have been made: 1) hysteresis is the dominating friction mechanism; 2) adhesion can be neglected due to the sliding velocities, pavement roughness and water film; 3) the contact conditions correspond to the boundary lubrication regime where in parts dry contact can be established; 4) viscous effects are insignificant compared to hysteretic effects; 5) the water acts as a coolant and ensures moderate tire temperatures compared to dry friction; 6) the water acts as a low-pass filter limiting the wavelengths the tire can follow in the high frequency range (sealing and expulsion constraints).

For lack of appropriate information about the rubber used in the W/S machine and as a first attempt to explore the potential of the theory of rubber friction for skid resistance prediction we utilized measured data of an actual tread rubber assuming that for an appropriate frequency band-temperature constellation a behavior similar to that of the Wehner/Schulze rubber could be found. The results seem to confirm this assumption. Nevertheless, further work should be based on the master curves of the measuring rubber instead. The master curves of the tread rubber are shown in Fig. 11 in terms of the storage (G') and loss modulus (G''). They apply to a temperature of 20 °C and a strain of 0.2%. However, the strain involved in skid resistance (e.g. W/S friction) measurement is much higher. A strain of 8% is considered a more

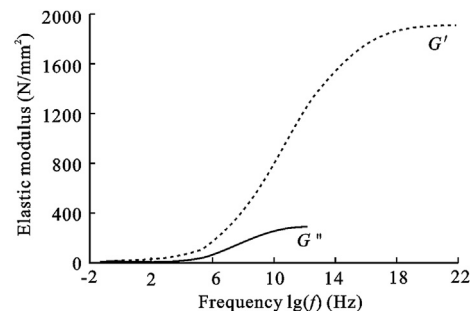


Fig. 11 – Measured storage (G') and loss modulus (G'') used for the rubber friction model ($T_0 = 20\text{ °C}$, $\epsilon = 0.2\%$).

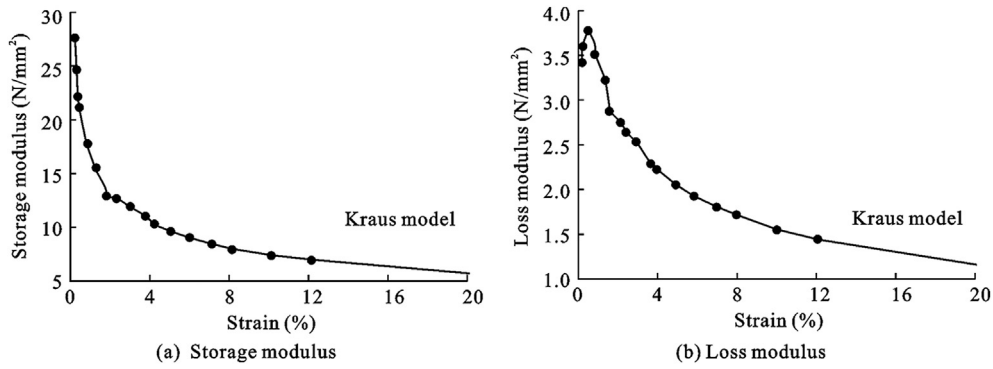


Fig. 12 – Measured strain dependence on storage and loss modulus for 10 Hz excitation frequency.



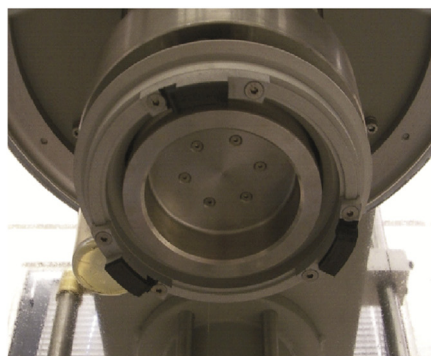
Fig. 13 – Wehner/Schulze (W/S) machine.

realistic magnitude for the tire-road contact (Persson, 2001b; Westermann et al., 2004). The modulus of elasticity is strongly dependent on the strain as described by Payne (1964). The effect of the strain on the modulus of elasticity of the tread rubber we used is shown in Fig. 12, measured at an excitation frequency of 10 Hz. The solid line is the so-called Kraus model (Kraus and Lansinger, 1992) fitted to the data. For our calculations we assumed that a characteristic strain of 8% and a softening effect according to Fig. 12 can be applied to the whole frequency range relevant to skid resistance (in our case about 103–106 Hz).

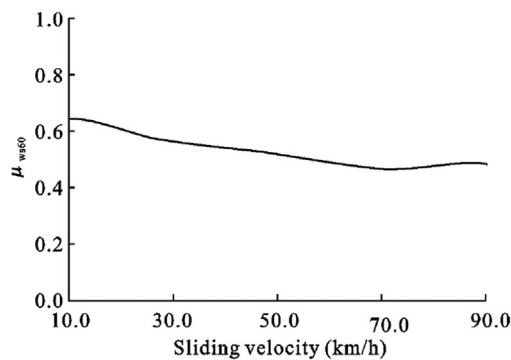
7. Experiments and results

The Wehner/Schulze (W/S) device (Fig. 13) was designed to simulate accelerated wear on road surface samples and measure the skid resistance before and after the accelerated testing. For the purpose of our investigation only the skid resistance measuring unit was used. It consists of a rotating head equipped with 3 rubber pads which are arranged equi-angular around a metal rim (Fig. 14(a)). For the skid resistance measurement the head is lifted from the pavement sample and accelerated to a rim speed of 100 km/h. When the desired speed is reached the water supply is activated and the rotating head released. It drops onto the pavement sample where it is decelerated due to the friction between rubber pads and specimen. The friction is recorded as a function of speed (Fig. 14(b)) and the friction coefficient at a speed of 60 km/h denoted the Wehner/Schulze friction coefficient μ_{ws60} . The nominal contact pressure is 0.2 N/mm² corresponding to a passenger car tire.

In order to validate the contactless skid resistance measurement the surface texture was measured under laboratory conditions by a chromatic white light sensor (Fig. 15(a)). The sensor features a lateral resolution of 1–2 μ m and a vertical resolution of 20 nm. For our investigations we limited the lateral resolution to 3.3 μ m. Because of the circular path of the Wehner/Schulze skid resistance measurement we measured the texture within or near the path of the Wehner/Schulze



(a) Skid resistance measuring unit



(b) Friction measurement

Fig. 14 – W/S machine.

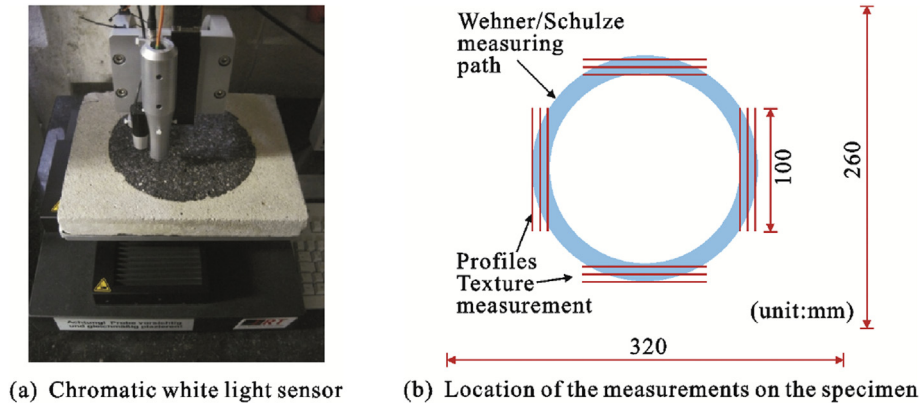


Fig. 15 – Measurement of surface texture.

device. The locations where the friction is measured can be seen from Fig. 15(b). 12 profiles with a length of 100 mm each were measured on every specimen. The profiles were subdivided into lengths of 25 mm (about 2–3 times, in some cases 5 times the wavelength of the macro-asperities) and then Fourier transformed. The 1D power spectral densities calculated were converted to 2D-PSDs and averaged assuming 2D isotropic surface roughness. Furthermore we found that it was crucial in this process that only the “summit texture” was considered in the calculation which is reasonable since the texture in the cavities does not contribute to hysteretic friction. For the surfaces investigated the “summit texture” conformed to the upper 33% of the surface texture on average but could differ between 20% and 45% in the particular case. The corresponding texture depths were found to be in close agreement with the respective theoretical penetration depths calculated according to Persson's contact theory.

In this study 33 different surfaces have been tested. 13 of them were washed concrete slabs made in the laboratory exhibiting different maximum aggregate sizes (8 and 11 mm) and different polishing treatments. 20 of them were asphalt cores obtained from actual road surfaces and parking lots comprising maximum aggregate sizes between 8 and 11 mm. Except for one sample which was an SMA, all of them were asphalt concrete (AC) pavements. Examples of the specimens are shown in Fig. 16. Two samples per surface were available for testing on average. The surfaces and corresponding friction data are listed in Table 1. For lack of space only a few photos are included in the table. They are just illustrative and

represent only a part of the variety of surfaces tested. The surfaces cover a wide range of friction coefficients from low- μ to high- μ roughness. Note that a Wehner/Schulze friction coefficient of around 0.6 marks a high- μ pavement because of the high sliding velocities and temperatures involved.

The concrete slabs made in the laboratory were subjected to sandblasting and subsequent polishing in two stages in order to enlarge the sample size. The respective surfaces are denoted accordingly in Table 1. The polishing was performed by the ARTe (Aachen rafeling tester) shown in Fig. 17. It features a pair of passenger car wheels which are moved across the specimen surface in a combined rotational and translational motion. The tires of dimension 165/75 R14 are operated with a tire pressure of 2 bar. The load is 1.500 N. A mixture of polishing agents and water was applied to accelerate the wear.

The results for the calculation of the W/S friction coefficients are given in Table 1. The comparison between measured and calculated friction coefficients is shown in Fig. 18(a). The macroscopic contact pressure was set to $\sigma_0 = 0.2 \text{ N/mm}^2$, Poisson's ratio to $\nu = 0.5$ and the maximum and minimum wavelengths to 25 mm and 20 μm respectively. The best agreement between calculated and measured friction coefficients was obtained with a background temperature (in the rubber) of 57 °C and a linear fit of the power spectral density in the log–log scale under the premise that only the wavelengths between 1 mm and 60 μm determine the fit. This means that wavelengths between 25 mm and 20 μm were included in the calculation of the friction coefficient,

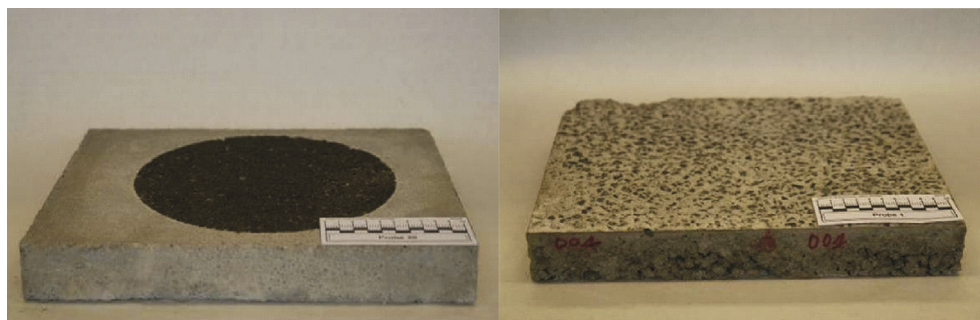
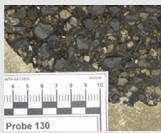


Fig. 16 – Examples of specimens tested: asphalt core and laboratory sample (concrete).

Table 1 – Surface samples tested for the comparison with the W/S machine.

No.	μ_{WS60} Measured	μ_{WS60} Theory	Number of samples	Surface example	Details/Origin
1	0.43	0.42	2		Exposed aggregate concrete, initial state
2	0.62	0.61	2		Exposed aggregate concrete, sandblasted
3	0.42	0.44	2		Exposed aggregate concrete, polishing stage 1
4	0.43	0.41	2		Exposed aggregate concrete, polishing stage 2
5	0.45	0.44	2		Exposed aggregate concrete, initial state
6	0.64	0.64	2		Exposed aggregate concrete, sandblasted
7	0.47	0.47	2		Exposed aggregate concrete, polishing stage 1
8	0.45	0.48	2		Exposed aggregate concrete, polishing stage 2
9	0.36	0.31	2		Exposed aggregate concrete, initial state
10	0.53	0.52	2		Exposed aggregate concrete, sandblasted
11	0.32	0.34	2		Exposed aggregate concrete, polishing stage 1
12	0.37	0.38	2		Exposed aggregate concrete, polishing stage 2
13	0.24	0.25	4		Aachen, Goethestraße 13
14	0.20	0.22	2		AC, Aachen, Boxgraben 22, initial state
15	0.18	0.17	2		AC, Aachen, Boxgraben 22, polishing stage 1
16	0.19	0.20	2		AC, Aachen, Boxgraben 22, polishing stage 2
17	0.17	0.20	4		AC, Aachen, Lütticher Straße 21
18	0.30	0.28	1		AC, Aachen, Wallstraße 57
19	0.30	0.29	2		AC, Aachen, Lütticher Straße 56, right lane
20	0.24	0.23	4		AC, Aachen, Lütticher Straße 56, left lane
21	0.28	0.28	1		AC, Aachen, Boxgraben 32
22	0.28	0.28	1		AC, Aachen, Lütticher Straße 21, bicycle lane
23	0.33	0.35	3		AC, Aachen, Rüd. Ring, road surface
24	0.50	0.55	3		AC, Aachen, Rüd. Ring, adjacent areas
25	0.36	0.38	1		AC, Aachen, Madrider Ring
26	0.30	0.27	2		SMA, Eschweiler (36 + 37), left and right lane
27	0.28	0.26	1		AC, Aachen, parking lot, coarse aggregate
28	0.31	0.29	2		AC, Aachen, parking lot, fine aggregate
29	0.32	0.30	2		AC, Aachen, parking lot
30	0.36	0.35	2		AC, Aachen, parking lot
31	0.33	0.34	2		AC, Aachen, parking lot
32	0.35	0.33	1		AC, Aachen, Schleidener Straße
33	0.46	0.47	4		Exposed aggregate concrete

however, wavelengths between 1 mm and 60 μm were considered decisive. As can be seen from the graph the agreement between measured and calculated friction coefficients is very good ($R^2 = 0.97$). The blue dots mark the

mean values of the 33 surfaces, the white dots the single values (70 in total). The 95% confidence bounds are shown in Fig. 18(b). At the waist the 95% prediction interval is ± 0.042 and the variance is 0.021.

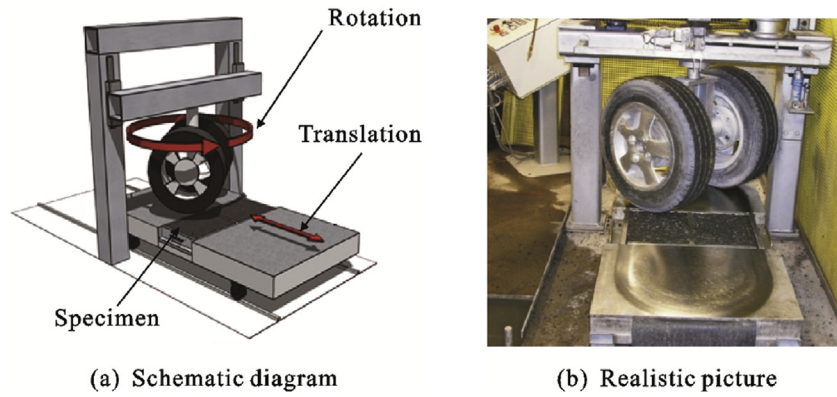


Fig. 17 – Aachen rafeling tester (ARTE).

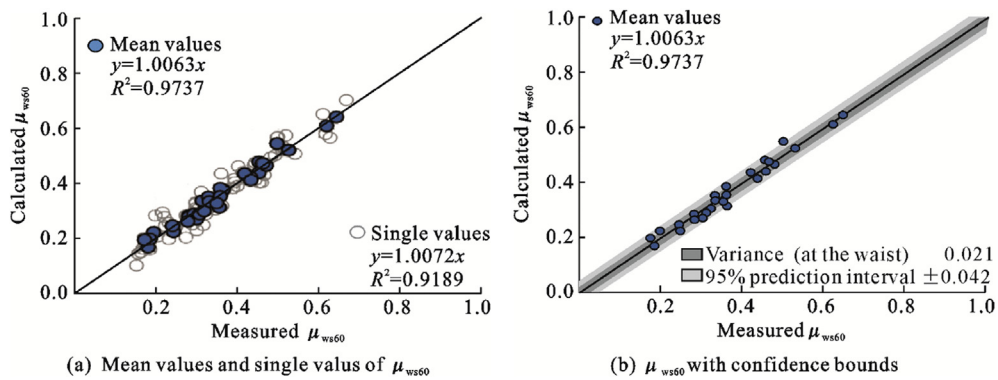


Fig. 18 – Comparison of measured and calculated friction coefficients.

The assumptions made seem to be quite reasonable; 60 °C is a typical tire temperature during driving on a dry road; on a wet road due to liquid cooling the temperature is typically around 30 °C. Thus, a rubber temperature of 57 °C can be expected as an average in the vicinity of contact spots under wet sliding conditions.

8. Conclusions

We have presented a concept of contactless skid resistance measurement. It consists of two components: 1) measurement of the pavement texture by means of an optical measuring system and 2) calculation of the skid resistance based on the measured texture by means of a rubber friction model. We described the basic assumptions underlying the theoretical approach and presented the model based on the theory of Persson. Further, we described the measurement devices and experiments conducted. For texture measurement we used a chromatic white light sensor. For lack of appropriate information about the particular measuring rubber and as a first attempt to explore the potential of the approach we utilized measured data of an actual tread rubber assuming that a certain temperature and strain behavior (WLF equation and Kraus model) could be attributed to the relevant frequency range (approximately 103–106 Hz). The results are promising. A close relation between measured and predicted friction coefficients could be found. The 95% prediction

interval is ± 0.042 and the variance is 0.021. Thus, a strong indication could be provided by the investigations that skid resistance could be measured without contact in the future. As a next step the contactless skid resistance measurements should be extended from laboratory environment to in-situ applications. This involves the setup of a new optical sensor and according data processing which is to be optimized in extensive testing on the road.

Acknowledgments

This study was conducted as part of a research project funded by the German Federal Ministry of Economy and Technology (No. 19S11002).

REFERENCES

Balmer, G., 1975. *The Significance of Pavement Texture*. FHWA-RD-75-12 Final Report. FHWA, Washington D C.

Barquins, M., Roberts, A.D., 1986. Rubber friction variation with rate and temperature: some new observations. *Journal of Physics D: Applied Physics* 19, 547–563.

Barquins, M., 1985. Sliding friction of rubber and Schallamach waves – a review. *Materials Science and Engineering* 73, 45–63.

- Ben Slimane, A., Khoudeir, M., Brochard, J., et al., 2008. Characterisation of road microtexture by means of image analysis. *Wear* 264, 464–468.
- Bowden, F.P., Tabor, D., 1966. Friction, lubrication and wear: a survey of work during the last decade. *British Journal of Applied Physics* 17, 1521–1544.
- Carbone, G., Lorenz, B., Persson, B.N.J., et al., 2009. Contact mechanics and rubber friction for randomly rough surfaces with anisotropic statistical properties. *The European Physical Journal E* 29, 275–284.
- Cigada, A., Mancosu, F., Manzoni, S., et al., 2010. Laser triangulation device for in-line measurement of road texture at medium and high speed. *Mechanical Systems and Signal Processing* 24 (7), 2225–2234.
- Descornet, G., Schmidt, B., Boulet, M., et al., 2006. FEHRL Report 2006/01, IFSTTAR Brussels Harmonization of European Routine and Research Measuring Equipment for Skid Resistance.
- Do, M.T., Marsac, P., Delanne, Y., 2004a. Prediction of tire/wet road friction from road surface microtexture, and tire rubber properties. In: 5th International Symposium on Pavement Surface Characteristics, Toronto, 2004.
- Do, M.T., Marsac, P., Mosset, A., 2004b. Tribology approach to predict the variation of tire/wet road friction with slip speed. In: 5th International Symposium on Pavement Surface Characteristics, Toronto, 2004.
- Do, M.T., Zahouani, H., 2005. Influence of the road-surface texture on the speed dependency of tire/road friction. In: 10th International Conference Metrology and Properties of Engineering Surfaces, Saint Etienne, 2005.
- Dunford, A., 2008. Measuring Skid Resistance without Contact, 2006–2007 Progress Report, Published Project Report PPR 315. Transport and Research Laboratory, Wokingham.
- Dunford, A., 2010. Measuring Skid Resistance without Contact, 2009–2010 Progress Report, Published Project Report PPR 538. Transport and Research Laboratory, Wokingham.
- El Gendy, A., Shalaby, A., Saleh, M., et al., 2011. Stereo-vision applications to reconstruct the 3D texture of pavement surface. *International Journal of Pavement Engineering* 12 (3), 263–273.
- Ergün, M., Iyınam, S., Iyınam, A.F., 2005. Prediction of road surface friction coefficient using only macro-and microtexture measurements. *Journal of Transportation Engineering* 131, 311–319.
- Forster, S.W., 1981. Aggregate Microtexture: Profile Measurement and Related Frictional Levels. FHWA-RD-81-107 Final Report. FHWA, Washington DC.
- Geyer, W., 1972. Der Einfluss geometrischer Reibflächen-Rauhigkeitsformen auf das trockene und nasse Reibverhalten von Gummi. *Automobil-Industrie*, I, 2/72: 41; II, 4/72: 39.
- Giles, C.G., 1957. The skidding-resistance of roads and the requirements of modern traffic. Road Paper No. 52. Proceedings of the Institution of Civil Engineers 6 (2), 216–242.
- Giles, C.G., 1965. The skid-resisting properties of wet surfaces at high speeds. *Journal of the Royal Aeronautical Society* 542, 83–94.
- Golden, J.M., 1981. A theory of wet road/tyre friction. *Wear* 71, 307–331.
- Goubert, L., Vuye, C., Jacobs, T., et al., 2010. Micro/macrotecture and skidding resistance. In: Tire Technology Expo 2010 & Conference, Koelnmesse, Cologne, 2010.
- Greenwood, J.A., Minshall, H., Tabor, D., 1961. Hysteresis losses in rolling and sliding friction. Proceedings of the Royal Society of London A 24 259 (1299), 480–507.
- Greenwood, J.A., Williamson, J.B.P., 1966. Contact of nominally flat surfaces. Proceedings of the Royal Society of London A 26 295 (1442), 300–319.
- Grosch, K.A., 1963. The relation between the friction and viscoelastic properties of rubber. Proceedings of the Royal Society of London A 274 (1356), 21–39.
- Heinrich, G., 1992a. Dynamics of carbon black filled networks, viscoelasticity and wet skid behaviour. *Kautschuk und Gummi, Kunststoffe* 45 (3), 173–180.
- Heinrich, G., 1992b. The dynamics of tire tread compounds and their relationship to wet skid behavior. *Progress in Colloid and Polymer Science* 90, 16–26.
- Heinrich, G., Klüppel, M., 2008. Rubber friction, tread deformation and tire traction. *Wear* 265, 1052–1060.
- Heinrich, G., Klüppel, M., Vilgis, T.A., 2000. Evaluation of self-affine surfaces and their implication for frictional dynamics as illustrated with a rouse material. *Computational and Theoretical Polymer Science* 10, 53–61.
- Holla, L., Yandell, W.O., 1973. A review of research on road-tyre friction. *Australian Road Research* (2) (Vermont).
- Holt, F.B., Musgrove, G.R., 1982. Surface texture classification: a guide to pavement skid resistance. In: Hayden, C.M. (Ed.), *Pavement Surface Characteristics and Materials*, pp. 31–44. ASTM STP 763.
- Horne, W.B., Bühlmann, F., 1983. A Method for Rating the Skid Resistance and Micro/macrotecture Characteristics of Wet Pavements. In: *Frictional Interaction of Tire and Pavement*, pp. 191–218. ASTM STP 793.
- Holla, L., 1977. Influence of Surface Texture on Road-tyre Friction. Highway Research Bulletin, New Delhi.
- Iaquinta, J., Fouilloux, A., 2003. A differential scattering probe for monitoring road surfaces. *Measurement Science Review* 3 (3), 107–110.
- Kane, M., Do, M.T., 2006. A contribution of elasto-hydrodynamic lubrication for estimation of tire-road friction in wet conditions. In: Aitc-ait 2006 International Conference on Tribology, Parma, 2006.
- Kazakov, A.L., 1986. Pavement texture and its wave-scattering properties: application to light reflectance and skid resistance. *Transportation Research Record* 1093, 48–57.
- Kebrle, J., Walker, R., 2007. Texture measurement and friction estimation using laser data acquisition and neural networks. In: Proceedings of the 9th WSEAS International Conference on Mathematical and Computational Methods in Science and Engineering, Trinidad and Tobago 2007.
- Klüppel, M., Heinrich, G., 2000. Rubber friction on self-affine road tracks. *Rubber Chemistry and Technology* 73 (578), 578–606.
- Kokkalis, A.G., Panagouli, O.K., 1998. Fractal evaluation of pavement skid resistance variations. I: surface wetting. *Chaos, Solutions and Fractals* 9 (11), 1875–1890.
- Kraus, G., Lansinger, C.M., 1992. Characterization of surface energy of carbon black surfaces and relationship to elastomer reinforcement. *Kautschuk Gummi Kunststoffe* 45, 459–468.
- Kummer, H.W., 1968. Lubricated friction of rubber discussion. *Rubber Chemistry and Technology* 41 (4), 895–907.
- Kummer, H.W., 1966. Unified theory of rubber and tire friction. *Engineering Research Bulletin* B-94.
- Kummer, H.W., Meyer, E., 1960. Rubber and tire friction. *Engineering Research Bulletin* B-80.
- La Torre, F., Domenichini, L., 2001. Friction prediction models. In: 2nd International Colloquium on Vehicle Tyre Road Interaction, Florence.
- Le Gal, A., Klüppel, M., 2008. Investigation and modeling of rubber stationary friction on rough surfaces. *Journal of Physics: Condensed Matter* 20, 13.
- Leu, M.C., Henry, J.J., 1978. Prediction of skid resistance as a function of speed from pavement texture measurements. *Transportation Research Record* 666, 7–13.

- Ludema, K.C., Tabor, D., 1966. The friction and viscoelastic properties of polymeric solids. *Wear* 9 (5), 329–348.
- Majumdar, A., Bhushan, B., 1990. Role of fractal geometry in roughness characterization and contact mechanics of surfaces. *Journal of Tribology* 112 (2), 205–216.
- Majumdar, A., Tien, C.L., 1990. Fractal characterization and simulation of rough surfaces. *Wear* 136 (2), 313–327.
- Meegoda, J.N., 2009. Non-contact Skid Resistance Measurement (Final Report New Jersey Institute of Technology, Newark).
- Moore, A.B., Humphreys, J.B., 1973. High speed skid resistance and the effects of surface texture on the accident rate. In: Hayden, C.M. (Ed.), *Skid Resistance of Highway Pavements*, pp. 91–100. ASTM STP 530.
- Moore, D.F., 1966. Prediction of skid resistance gradient and drainage characteristics for pavements. *Highway Research Records* 131, 181–203.
- Moore, D.F., 1969. A history of research on surface texture effects. *Wear* 13 (6), 301–312.
- Moore, D.F., 1980. Friction and wear in rubbers and tyres. *Wear* 61 (2), 273–283.
- Moore, D.F., Geyer, W., 1974. A review of hysteresis theories for elastomers. *Wear* 30 (1), 1–34.
- Mu, X.Y., Li, L., Tang, N., et al., 2003. A laser-based system for highway pavement texture measurement. In: *Proceedings of the Conference on Intelligent Transportation Systems*, Shanghai, 2003.
- Moore, D.F., 1972. *The Friction and Lubrication of Elastomers*. Pergamon Press, Oxford.
- Moore, D.F., 1975. *The Friction of Pneumatic Tires*. Elsevier Scientific Company, Amsterdam.
- Payne, A.R., 1964. Strainwork dependence of filler-loaded vulcanizates. *Journal of Applied Polymer Science* 8 (6), 2661–2686.
- Persson, B.N.J., 2000. *Sliding Friction, Physical Principles and Applications*. NanoScience and Technology, second ed. Springer, Berlin-Heidelberg.
- Persson, B.N.J., 2001a. Theory of rubber friction and contact mechanics. *Journal of Chemical Physics* 115 (8), 3840–3861.
- Persson, B.N.J., 2001b. Theory of rubber friction, contact mechanics and the role of surface roughness on the adhesion of elastic solids. In: *160th Meeting of the Rubber Division, American Chemical Society*, Cleveland, 2001.
- Persson, B.N.J., 2006a. Contact mechanics for randomly rough surfaces. *Surface Science Reports* 61, 201–227.
- Persson, B.N.J., 2006b. Rubber friction: the role of the flash temperature. *Journal of Physics: Condensed Matter* 18, 7789–7823.
- Persson, B.N.J., 2007. Relation between interfacial separation and load: a general theory of contact mechanics. *Physical Review Letters* 99, 14.
- Persson, B.N.J., 2011a. Fluid squeeze-out between rough surfaces: comparison of theory with experiment. *Journal of Physics: Condensed Matter* 23, 9.
- Persson, B.N.J., 2011b. Rubber friction and tire dynamics. *Journal of Physics: Condensed Matter* 23, 14.
- Persson, B.N.J., Albohr, O., Tartaglino, U., et al., 2001. On the nature of surface roughness with application to contact mechanics, sealing, rubber friction and adhesion. *Journal of Physics: Condensed Matter* 17, 3840–3861.
- Persson, B.N.J., Lorenz, B., Volokitin, A.I., 2010. Heat transfer between elastic solids with randomly rough surfaces. *The European Physical Journal E* 31, 3–24.
- Persson, B.N.J., Tartaglino, U., Tosatti, E., et al., 2004. Rubber friction on wet rough substrates at low sliding velocity: the sealing effect. *Kautschuk Gummi Kunststoffe* 57 (10), 532–537.
- Persson, B.N.J., Tartaglino, U., Albohr, O., et al., 2005. Rubber friction on wet and dry road surfaces: the sealing effect. *Physical Review B* 71, 7.
- Pinnington, R.J., 2009. Rubber friction on rough and smooth surfaces. *Wear* 267 (9/10), 1653–1664.
- Pinnington, R.J., 2012. A particle-envelope surface model for road-tyre interaction. *International Journal of Solids and Structures* 49, 546–555.
- Radó, Z., 1994. *A Study of Road Surface Texture and its Relationship to Friction*. Pennsylvania State University University park. Ph.D thesis.
- Rhode, S.M., 1976. On the effect of pavement microtexture and thin film traction. *International Journal of Mechanical Sciences* 18 (2), 95–101.
- Roberts, A.D., 1992. A guide to estimating the friction of rubber. *Rubber Chemistry and Technology* 65 (3), 673–686.
- Sabey, B.E., Lupton, G.N., 1967. *Measurement of Road Surface Texture Using Photogrammetry*. Report LR 57, Road Research Laboratory, Wokingham.
- Savkoor, A.R., 1965. On the friction of rubber. *Wear* 8 (3), 222–237.
- Schallamach, A., 1953. The load dependence of rubber friction. *Rubber Chemistry and Technology* 26 (2), 297–301.
- Schonfeld, R., 1970. *Skid Numbers from Stereo-photographs*. Report RR 155, Ontario Department of Highway Toronto.
- Schulze, C., 2011. *Ein geometrisch basiertes Modell zur Ableitung von Reibwerten bei Nässe aus der Textur*. Ph.D Thesis. RWTH Aachen University, Aachen.
- Schulze, K.H., 1959. Einfluss der geometrischen Feingestalt der Straßenoberfläche auf den Kraftschluss. *Straße und Autobahn* 10 (10), 379.
- Schulze, K.H., 1969. Zur quantitative Bewertung der Rauheit von Straßenoberflächen in Beziehung zum Reibungswiderstand bei Nässe. *Technical University of Berlin, Berlin*. Ph.D thesis.
- Schulze, K.H., 1970. Typen der Oberflächenfeingestalt und ihre Wirkung auf den Reibungs-widerstand bei Nässe. In: *Internationales Colloquium über Straßengriffigkeit und Verkehrssicherheit bei Nässe*, Berlin, *Berichte des Institutes für Straßen- und Verkehrswesen*, Heft 2, Berlin/München, 1970.
- Schulze, K.H., 1979. Griffigkeit und rauheit. In: Wehner, Schulze, Siedek (Eds.), *Handbuch des Straßenbaus*, Bd. 1. Springer-Verlag, Berlin-Heidelberg.
- Shalaby, A., El Gendy, A., 2008. Three-dimensional pavement surface macrotexture measurements using the photometric stereo technique and applications. In: *6th International Symposium on Pavement Surface Characteristics SURF 2008*, Portoroz, 2008.
- Spring III, W.C., King, W.L., 1981. Light Depolarization as a Measure of Pavement Surface Texture. *Final Report. Naval Surface Weapons Center, Silver Spring*.
- Tabor, D., 1967. Solid friction and boundary lubrication. *Proceedings of the Institution of Mechanical Engineers* 182 (1), 262–280.
- Taneerananon, P., Yandell, W.O., 1981. Microtexture roughness effect on predicted road-tyre friction in wet conditions. *Wear* 69 (3), 321–337.
- Ustuntas, T., 2007. Prediction of skid resistance coefficient of cement concrete roads with fuzzy logic. *Civil Engineering and Environmental Systems* 24 (3), 233–246.
- Wambold, J.C., Antle, C.E., Henry, J.J., et al., 1995. *International Experiment to Compare and Harmonize Skid Resistance and Texture Measurements*. PIARC Report 01.04.T., PIARC, Paris.
- Wambold, J.C., Henry, J.J., Hegmon, R.R., 1982. Evaluation of pavement surface texture significance and measurement techniques. *Wear* 83 (2), 351–368.
- Wang, D., Ueckermann, A., Schulze, C., et al., 2012. *Berührungslose Griffigkeitsmessung*. Forschungsbericht. RWTH Aachen University, Aachen.
- Westermann, S., Petry, F., Boes, R., et al., 2004. *Experimental investigations into the predictive capabilities of current*

- physical rubber friction theories. *Kautschuk Gummi Kunststoffe* 57 (12), 645–650.
- Williams, M.L., Landel, R.F., Ferry, J.D., 1955. The temperature dependence of relaxation mechanisms in amorphous polymers and other glass-forming liquids. *Journal of the American Chemical Society* 77 (14), 3701–3707.
- Xie, L., Chu, X., Wang, W., et al., 2009. A stereoscopic imaging arithmetic for 3D measurement of road surface microtexture. In: *Proceedings of the International Conference on Transportation Engineering, Chengdu, 2009*.
- Xie, J., Liu, R., Michalk, B., 2008. Automatic skid number evaluation using texture laser measurement. In: *International Conference on Networking, Sensing and Control, ICNSC 2008, Sanya, 2008*.
- Yandell, W.O., 1971. A new theory of hysteretic sliding friction. *Wear* 17 (4), 229–244.
- Yandell, W., Taneerananon, P., Zankin, V., 1983. Prediction of Tire-road Friction from Surface Texture and Tread Rubber Properties. In: *Frictional Interaction of Tire and Pavement*, pp. 304–322. ASTM STP 793.
- Yang, C., Persson, B.N.J., 2008. Contact mechanics: contact area and interfacial separation from small contact to full contact. *Journal of Physics: Condensed Matter* 20, 13.
- Zahouani, H., Vargiolu, R., Do, M.T., 2000. Characterization of microtexture related to wet road/tire friction. In: *4th International Symposium on Pavement Surface Characteristics SURF 2000, Nante, 2000*.